Nanoscale

This is an *Accepted Manuscript*, which has been through the Royal Society of Chemistry peer review process and has been accepted for publication.

Accepted Manuscripts are published online shortly after acceptance, before technical editing, formatting and proof reading. Using this free service, authors can make their results available to the community, in citable form, before we publish the edited article. We will replace this *Accepted Manuscript* with the edited and formatted *Advance Article* as soon as it is available.

You can find more information about *Accepted Manuscripts* in the **Information for Authors**.

Please note that technical editing may introduce minor changes to the text and/or graphics, which may alter content. The journal's standard **Terms & Conditions** and the **Ethical guidelines** still apply. In no event shall the Royal Society of Chemistry be held responsible for any errors or omissions in this *Accepted Manuscript* or any consequences arising from the use of any information it contains.

Journal Name

ARTICLE

Ceria loaded nanoreactors: a nontoxic superantioxidant system with high stability and efficacy

M. Spulber,[a] P. Baumnn,[a] J. Liu, [a] and C.G. Palivan[a*]

Medical applications of the superantioxidant ceria nanoparticles (CeNP) are limited by their high toxicity and low stability. CeNP toxicity is related to its aggregation in solution, and the possible generation of reactive oxidative species (ROS) by a Fenton-like reaction. For efficient medical applications it is necessary to find new solutions, which simultaneously reduce CeNP inherent toxicity while preserving their unique catalytic regenerative qualities. Here we introduce a straightforward strategy based on CeNP encapsulation in polymer vesicles which reduces their toxicity, but preserves their superantioxidant character. We have engineered antioxidant nanoreactors, which serve the dual role of: (i) separation of CeNP particles, which inhibits aggregate formation, and (ii) protection of CeNP from hydrogen peroxide, thus eliminating the Fenton-like reaction which induces cytotoxicity. Nanoreactors containing CeNP possess a higher scavenging activity than free CeNP for both hydroxyl and superoxide radicals, as indicated by spin trapping EPR. Due to the regenerative redox chemistry of ceria, the nanoreactors are active for long periods of time, without requiring additional reducing agents. Upon uptake by cells, the nanoreactors show almost no toxicity compared with free CeNP after long term exposure, thus proving their high efficacy as ROS scavengers. Our strategy of engineering CeNP-containing nanoreactors represents a versatile, simple and economical solution to reduce CeNP toxicity, while preserving their functionality; thus nanoreactors are ideal candidates for fighting oxidative stress in a large variety of medical situations.

Introduction

Oxidative stress induces an imbalance of reactive oxygen species (ROS), which may overwhelm cellular defences that are regulated by a plethora of molecules with antioxidant activity (glutathione, ascorbate, glutathione peroxidase, glutathione transferase, superoxide dismutase or catalase), [1] and thus cause toxicity effects. Due to the impact of oxidative stress in a variety of pathologic conditions, there are now significant efforts to identify efficient solutions to fight against diseases such as cancer, atherosclerosis, Parkinson's disease, Alzheimer's disease, diabetes, inflammation, or neurodegeneration [2,3]. One of the most efficient strategies based on nanoscience concepts has proved to be the design of nanoreactors by encapsulation in polymer vesicles of antioxidant enzymes, such as superoxide dismutase, [4,5] hemoglobin, [6] superoxide dismutase and lactoperoxidase, [7,8] or superoxide dismutase mimics [9]. Nanoreactors represent compartments with nanometer sizes in which defined chemical reactions take place [10,11,12,13]. They are designed to contain within their architecture the desired catalysts (enzymes, proteins, mimics or combinations of thereof), which are shielded from environmental degradation, while acting *in situ* [14,6,15]. Compared to conventional drug delivery systems in which the antioxidant compounds are active upon release [16], the use of nanoreactors has the advantage of maintaining *in situ* antioxidant activity for long periods of time, because of the

shielding effect of polymer vesicles. However, a reduced encapsulation efficiency of enzymes due either to inherent low solubility or to the statistical co-encapsulation process represents a limiting factor that is still to be addressed. While improved encapsulation efficiency is obtained by encapsulation in nanoreactors of small molecular mass mimics, [6] the intrinsic activity of mimics is lower than the corresponding enzymes. To the best of our knowledge, the combined effect of high encapsulation efficiency and highly active compounds has not been yet solved.

Ceria nanoparticles (CeNP) have been used as superantioxidant systems in various domains, ranging from material engineering and the car industry to electrolytic material for solid oxide fuel cells [17,18,19]. CeNP are based on ceria (CeO_2), a cubic fluorite type oxide whose catalytic activity is due to repetitive cycling between the Ce^{4+} and Ce^{3+} oxidation states. Oxygenation-deoxygenation cycles without disruption of the fluorite lattice-structure [20] allow scavenging of free radical species with high efficacy, and requires very little energy [18,21,19,22]. The efficiency of ceria particles is determined by the increase in lattice parameters with decreasing particle size, which induces specific control of oxygen vacancies and determines their reactivity [23]. This ability of CeNP to participate in redox coupled reactions makes them promising candidates for biological and medical applications, [24] as reported previously for protection from radiation-induced cellular damage, [25] nerve cell protection, [26] hepato-protection against monocrotaline hepatotoxicity, and prevention of cardiovascular myopathy [27, 28].

However, recent reports have indicated that CeNP lead to oxidative stress and DNA damage, and in high doses promote radical formation, via a possible Fenton-like reaction [29,30,31,32]. Incubation with CeNP induced cytotoxicity and genotoxicity after 72 h in HeLA cells, [33,34] hepatic toxicity, [35] pulmonary and extrapulmonary toxicity, [36] and neurotoxic effects due to depletion of serotonine [37]. Various factors, including synthetic routes, composition, purity, particle size, surface charge, and the use of non-stabilized CeNP for in vitro studies [24] have been suggested as possible causes of their toxicity. In addition, possible CeNP aggregation in solution is responsible for a decrease in scavenging efficiency [22]. Thus it is only by avoiding the CeNP toxicity and aggregation problems, whilst preserving their superantioxidant activity that effective solution can be found for the use of CeNP in the medical domain.

In this paper, we introduce a strategy based on CeNP encapsulation in polymer nanoreactors (Figure 1) for simultaneously preserving the superantioxidant activity of CeNP, whilst preventing their aggregation and interaction with H_2O_2, and decreasing their toxicity without further particle stabilization.
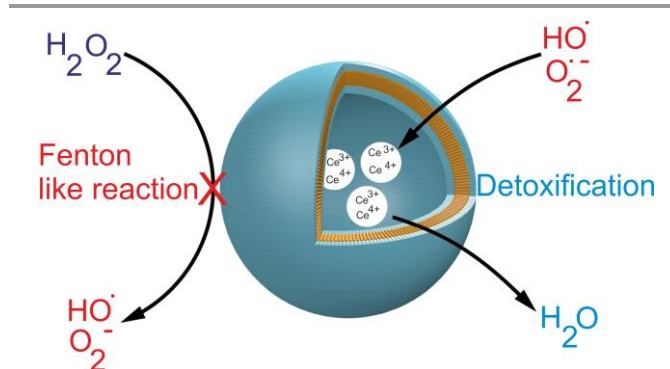

Figure 1 Schematic representation of CeNP nanoreactors based on CeNP encapsulation inside polymer vesicles for detoxification of ROS, without generation of new species by a Fenton like reaction.

We chose to assemble nanoreactors from poly(*N*-vinylpyrrolidone)-*block*-poly(dimethylsiloxane)-*block*-poly(*N*-vinylpyrrolidone) (PDMS-PNVP) block copolymers, which were expected to generate vesicles with a membrane permeable to O_2 and ROS, as previously reported for other PDMS based copolymer vesicles [14,6]. Polymer vesicles obtained by self-assembling amphiphilic block copolymers represent efficient compartments for the encapsulation of active compounds and the design of nanoreactors [38]. They have the advantages of membranes with higher mechanical stability than lipid-based vesicles (liposomes), while preserving low immunogenicity [12]. The CeNP encapsulated inside polymer vesicles benefit from the shielding effect of the polymer membrane, which limits interaction with H_2O_2, and prevents interactions which lead to aggregation of nanoparticles. Inside the cavity of vesicles CeNP can actively regenerate, and scavenge various free radical species, which pass through the polymer membrane. The ability of CeNP nanoreactors to scavenge different ROS was followed by spin trapping EPR, while the stability of the polymer membrane to hydrogen peroxide was followed by UV-vis spectroscopy. Uptake of CeNP nanoreactors was studied on HeLa cells by flow cytometry, and confocal laser scanning microscopy, and its cytotoxicity was assessed by the MTS assay. In vitro activity of CeNP nanoreactors was established on cells exposed to oxidative stress induced by paraquat. Thus the combination of superantioxidant CeNP with polymer vesicles to generate nanoreactors represent an efficient strategy for fighting oxidative stress because it benefits from the unique regenerative activity of CeNP, while preventing aggregation and ROS generation via Fenton like reaction with H_2O_2, the two main causes of CeNP toxicity.

Materials and Methods

Materials

4,4'-azobis(4-cyanovaleryl) chloride was synthesized by the reaction of 4,4'-azobiscyanopentanoic acid previously dried by azeotropic distillation from toluene, with phosphorus pentachloride (PCl_5) according to the method reported in the

literature [39] (Sigma-Aldrich). 1-Vinyl-2-pyrrolidinone (Sigma-Aldrich) was purified before use by vacuum distillation and kept under N_2. Chloroform (Sigma-Aldrich) was dried over P_2O_5 and purified by distillation. Toluene (Sigma-Aldrich) was distilled over Na wire. Octamethylcyclotetrasiloxane (D4; Sigma-Aldrich) and 1,3-bis(3-aminopropyl)-1,1,3,3-tetramethyldisiloxane (Alfa-Aesar) were used as received. Cerium oxide (CeO_2) with average size around 25 nm, hypoxanthine (HX), xanthine oxidase 1 U mL^{-1} (XOD), diethylene triamine pentaacetic acid (DTPA), hydrogen peroxide (H_2O_2), 5,5-dimethyl-1-pyrroline N-oxide (DMPO), and Sepharose 2B, were purchased from Sigma-Aldrich and used as received. Doxorubicin was purchased from Beijing Zhongshuo Pharmaceutical Technology Development Co., Ltd. and was used as received. 10 mM phosphate saline buffer (PBS) (pH 7.4, 136 mM NaCl, 2.6 mM KCl) was prepared by dissolving 8 g NaCl, 0.2 g KCl, 1.44 g Na_2HPO4 and 0.24 g of KH_2PO4 in 800 mL ddH_2O, adjusting the pH to 7.4 with HCl, and completing the volume to 1 L.

Synthesis of triblock copolymers

The synthesis of amphiphilic PDMS-PNVP triblock copolymers was previously described [40]. Two different PDMS-PNVP triblock copolymers (Scheme 1) were obtained starting from two α,ω-bis(aminopropyl) poly(dimethylsiloxane) (H_2N-PDMS-NH_2), with 17 and 37 siloxane units. The two H_2N-PDMS-NH_2 siloxanes were synthesized by equilibrium polymerization of D4 and APTES in the presence of the catalyst tetramethylamonium siloxanolate. Further, by condensation of H_2N-PDMS-NH_2 with 4,4-azobiscyanovaleryl chloride polydimethylsiloxanes with azo end groups were obtained. They were used as macroinitiators for radical polymerizations of N-vinylpyrrolidone, yielding two different PDMS-PNVP triblock copolymers (Scheme 1 and Table 1).
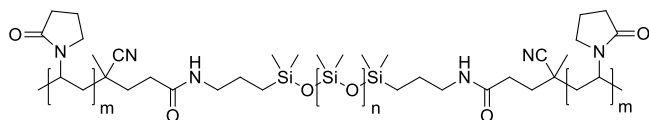
Scheme 1. PDMS-PNVP triblock copolymer

^{1}H-NMR (400.1 MHz, CDCl$_3$) δ/ppm = 3.7-3.85 (CH$_2$-*CH*-N), 3.0-3.2 (CH$_2$-*CH$_2$*-N-CO), 2.7-3.0 (CH$_2$-*CH$_2$*-CONH) 2.3-2.4 (CH$_2$-CH$_2$-*CH$_2$*-CO), 1.5-2.0 (*CH$_2$*-CH-N-CO, CH$_2$-*CH$_2$*-CH$_2$-CO, CH$_2$-CH$_2$-CO*NH*, *CH$_2$*-CH$_2$-C, CH$_2$-*CH$_2$*-C, CH$_2$-CH$_2$-C(*CH$_3$*)-CN), 1.45-1.50 ppm (CH$_2$-*CH$_2$*-CH$_2$), 0.54 (m, -Si*CH$_2$*), 0.1 (Si-*(CH$_3$)$_2$*).

The degree of polymerisation of the siloxane sequence (DP siloxane) was established from ^{1}H-NMR spectra of H_2N-PDMS-NH_2 synthesized in the first step. The degree of polymerisation of the vinyl sequence was calculated from the ^{1}H-NMR spectra of the three block copolymers with the relationship DP vinyl = DP siloxane*vinyl/siloxane molar ratio (Table 1).

Table 1. Characteristics of PDMS-PNVP triblock copolymers.

Polymer	DP siloxane block (n)	DP vinyl block (m)	Vinyl/siloxane molar ratio	M_n (GPC)	M_w/M_n	$F = M_n$ vinyl $/M_n$ siloxane
PDMS-PNVP1	17	17	1/1	4198	1.52	1.34
PDMS-PNVP2	37	30	0.8/1	6161	1.54	1.14

^{1}H-NMR spectra were recorded on a Bruker DPX-400 spectrometer operated at 400 MHz in CDCl$_3$ and processed with MestReNova software. Chemical shifts are reported in ppm relative to tetramethylsilane.

Gel permeation chromatography (GPC) was used in order to determine the average molecular weight M_n of the polymers and their polydispersity index (PDI). These parameters were determined using a Viscotek GPC max system equipped with four Polymer Agilent PL gel columns (10 µm guard; mixed C; 10 µm, 100 Å; 5 µm, 10^3 Å), using chloroform as eluent at a flow rate of 1mL min^{-1} at 40 °C. Signals were recorded with a refractive-index detector (RI) and calibrated against polystyrene standards (Agilent).

Preparation of CeNP nanoreactors

CeNP nanoreactors were formed using the film rehydration method [41]. First, 1 mL of a 5 mg mL^{-1} solution in ethanol of PDMS-PNVP copolymers was slowly evaporated in a rotary vacuum evaporator at reduced pressure until a film formed on the flask wall. This polymer film was then rehydrated i. in PBS for 12 hours under magnetic stirring (to obtain empty polymersomes) ii. with a solution of 0.1 mM CeNP (to obtain loaded nanoreactors) and iii. a mixture of 0.5 mg/mL doxorubicin and 0.1 mM CeNP (to obtain co-encapsulated doxorubicin and CeNP- containing polymersomes for the study of the cellular uptake). After rehydration the solutions were extruded through 200 nm track edge polycarbonate filters (Whatman). The nanoreactors containing only encapsulated CeNP were separated by size exclusion chromatography (SEC) through a Sepharose 2B column. The CeNP content inside nanoreactors was determined by UV-Vis spectroscopy (absorbance at 320 nm characteristic for Ce^{4+}), using an extinction coefficient of 9 x 10^{-5} M^{-1} cm^{-1} determined experimentally in PBS.

EPR samples preparation for generation, trapping and decay profile of hydroxyl radicals in presence of free and encapsulated CeNP

In order to monitor the changes in hydroxyl radical (HO$^·$) concentrations, DMPO was used as a spin trap. DMPO actively traps HO$^·$ to form DMPO/OH adducts which are paramagnetic,

so detectable by EPR spectroscopy. Hydroxyl radicals were generated by a Fenton reaction by mixing 20 μl 1 mM $FeSO_4$ and 20 μl 10 mM H_2O_2 with 140 μl PBS, and were trapped by addition of 20 μl 1 M DMPO as reported in the literature [42]. The samples containing free CeNP by mixing 100 μl free CeNP (concentration ranging from 0.03 to 5 mM) with 20 μl 1mM $FeSO_4$ and 20 μl 10 mM H_2O_2 ($HO^.$ generation) in 40 μl PBS. In order to spin trap $HO^.$ 20 μl 1 M DMPO were added in the last step of sample preparation. The samples containing CeNP nanoreactors were prepared in a similar manner by mixing 100 μl CeNP nanoreactors with 20 μl 1mM $FeSO_4$, 20 μl 10 mM H_2O_2, and 20 μl 1 M DMPO in 40 μl PBS. All the mixtures were incubated for 10 min before measuring their EPR spectra. In the measured solutions the final concentration of CeNP varied from 2.5 to 0.015 mM.

The ability of CeNP to generate hydroxyl radicals in a Fenton like reaction with hydrogen peroxide was tested by mixing 100 μl CeNP solution (5 mM or 0.03 mM) with 20 μl H_2O_2 (10 mM) and 20 μl 1 M DMPO in 60 μl PBS.

EPR sample preparation for generation, trapping and decay profile of superoxide radicals in presence of free and encapsulated CeNP

DMPO superoxide adducts (DMPO/OOH) were generated by a modification of previously published protocols [43]. Briefly, 20 μl 1 M DMPO was mixed with 100 μl 1 mM HX, 10 μl XO (to generate continuous superoxide radicals $O_2^{.-}$), and 70 μl PBS. DMPO superoxide adducts were generated in the presence of free and encapsulated CeNP by mixing 50 μl CeNP (0.018 to 3.75 mM) with 100 μl 1 mM HX, 10 μl XO ($O_2^{.-}$ generation), with DMPO (for spin trapping) and 20 μl PBS. All the samples were incubated for 10 min before measurement to achieve the maximum intensity of DMPO-OOH.

Viability assay

HeLa cells were seeded in 200 μL DMEM culture medium containing 10% FCS and 2 % Pen Strep antibiotics at a density of 2 x 10^4 cells per well in a 96 well plate and incubated for 24 h at 37°C and 5% CO_2. Cells were then incubated in 140 μL DMEM culture medium for another 24 h in the presence of 60 μL CeNP loaded nanoreactors or free CeNP in PBS. The media was then removed, the cells washed with PBS, and fresh media and 20 μL MTS assay solutions (Promega) were added, and incubated for another 2 h. The absorbance at 490 nm was measured using a well plate reader (SpectraMax) and normalized against control cells to determine 100% viability. Background corrections were made based on media incubated with the MTS assay solution.

Cellular uptake and in vivo stability experiment

HeLa cells were cultured at a density of 5x10^4 cells per well in an 8-well Lab-Tek plate (Nalge Nunc International, USA) for 24h in DMEM culture medium. Afterwards, 100 μg/ml PDMS-PNVP1-CeNP or PDMS-PNVP2-CeNP nanoreactors (considering the polymer concentration) were incubated in the presence of the cells for additional 24 h. Then, the cells were

stained with Hoechst 3342 (5mg/ml) and Cell mask Deep Red (5 mg/ml) for 10 min and 5 min, respectively. After rinsing with PBS, cells were imaged with a confocal laser scanning microscope (Carl Zeiss LSM510, Germany) equipped with a 63x water emulsion lens (Olympus, Japan). The confocal laser scanning microscopy (CLSM) micrographs were recorded in multitrack mode and the setting (gain and contrast) of each fluorescent dye was adjusted individually: Hoechst 3342 was excited at 405 nm in channel 1, Deep Red at 633 nm in channel 2 and Doxorubicin at 543 nm in channel 3. The images were recorded using Carl Zeiss LSM software (version 4.2 SP1). Control micrographs were recorded with the same settings as the sample images.

Cellular uptake was quantified by flow cytometry analysis. 1x10^5 HeLa cells were seeded in DMEM culture medium in a 24-well plate and cultured for 24 h at 37°C in a humidified CO_2 incubator. After 24h the medium was exchanged and replaced with fresh medium containing 100 μg/ml doxorubicin-containing CeNP-nanoreactors (PDMS-PNVP1-CeNP (0.0036 mM CeNP), PDMS-PNVP1-CeNP (0.003 mM CeNP), respectively). Doxorubicin was co-encapsulated together with CeNPs as a fluorescent marker for the cellular uptake of the nanoreactors. For flow cytometry cells were washed with PBS, trypsinized, centrifuged, resuspended in 1 ml of PBS and put on ice. Flow cytometry was measured with a flow cytometry setup (BD Bioscience, USA) by analysing the fluorescent signal of doxorubicine of a total of 10,000 cells for each condition. Data were processed using Flowing Software 2.5.0 (Turku Centre for Biotechnology, Finland).

Cell viability in the presence of ROS source

HeLa cells were incubated with CeNP nanoreactors as described above for the flow cytometry experiment. After 24 h incubation with CeNP nanoreactors, the cell medium was exchanged and replaced by fresh medium containing 2mM paraquat to induce ROS in the cell. To determine viability, cells were stained with propidium iodide (PI, 50 μg/ml) [7] and flow cytometry measurements were performed. Control cell stained with PI was considered as 100% viable.

Methods

Dynamic and static light scattering (DLS, SLS) were used to determine the sizes of the free CeNP and CeNP containing nanoreactors. Measurements were performed on an ALV (Langen, Germany) goniometer, equipped with an ALV He-Ne laser (λ = 632.8 nm) using serial dilutions to produce polymer concentrations ranging from 0.12 to 2 mg/mL. Light scattering was measured in 10 mm cylindrical quartz cells at angles between 30 and 150° at 293 K. The photon intensity auto correlation function g2(t) was determined with an ALV-5000E correlator. Data were processed using ALV static & dynamic fit and plot software (version 4.31 10/01). SLS data were processed according to the Guinier-model and DLS data by using a Williams-Watts function.

Transmission electron microscopy (TEM) was used for characterization of the morphology of free CeNP and CeNP nanoreactors. Measurements were performed on a Philips EM400 electron microscope operating at 100 kV. Polymersome dispersions were deposited on a carbon-coated copper grid and negatively stained with 2% uranyl acetate solution.

UV-Vis spectroscopy was used to determine the concentration of Ce^{4+} in various CeNP samples. Absorption spectra were measured in 1 cm quartz and silica glass cuvettes (Hellma) using a Specord 210 plus spectrometer (Analytik Jena, Germany) with a slit width of 4 nm. In order to determine CeNP concentrations in samples of loaded polymersomes, the absorption was measured at 320 nm, which is characteristic for Ce^{4+} [19]. An extinction coefficient of 9 x 10^{-5} M^{-1} cm^{-1} (determined experimentally by a dilution series in PBS) was used.

Electron paramagnetic resonance (EPR) measurements were performed on a Bruker CW EPR Elexsys-500 spectrometer equipped with a variable temperature unit. Spectra were recorded at 298 K with the following parameters: microwave power 2 mW, conversion time 30 ms, number of scans up to 20, resolution 2048 points, modulation amplitude 1 G, sweep width 100 G. The hyperfine couplings of the spin adducts were determined by simulating the spectra using the WinSim (NIEHS/NIH) simulation package [44]; for spectra that consisted of a superposition of contributions from different adducts or radicals, the fitting also determined the relative intensity of each component with a typical margin of error of 5% in multicomponent spectra.

FTIR spectra were recorded on a Bruker Alpha FTIR spectrometer (Bruker Optic GmbH, Ettlingen, Germany) to show the structure of CeNP.

X-ray Diffraction (XRD) Measurements were performed on a Siemens D5000 diffractometer using Cu Kα radiation generated at 40 kV and 30 mA. Samples were scanned with scan rate of 0.020°/step in the range of $2\theta = 20\text{-}80°$ and 1 s/step. The Debye-Scherrer equation was applied to calculate crystallite diameters.

$d_{XRD} = K\,\lambda/\,\beta\,\cos\theta$ (1), where d_{XRD} is the crystallite diameter, K is a constant estimated as 0.941, λ is the wavelength of radiation, β is the peak width at half height in radians, and θ is the angle of reflection.

Result and discussion

We engineered nanoreactors by encapsulation of CeNP inside polymer vesicles in order to solve their toxicity issues, by avoiding aggregation in solution and shielding them from H_2O_2, while preserving their ability to scavenge free radicals. The effectiveness of this procedure is described below.

Characterization of CeNP

First, we characterized CeNP by a combination of XRD, FTIR, DLS and TEM. XRD powder spectrum of CeNP indicated (111), (200), (220), (311), (400), (331), (420) and (422)

reflections (Figure S1A), which correspond to the polycrystalline cubic structure of CeO_2 [45]. As expected, CeNP gives isolated narrow peaks in XRD due to its cubic fluorite structure [23]. The crystallite size was calculated based on Scherrer's equation (1), and was equal to 20 nm.

FT-IR spectrum of CeNP (Figure S1B) shows the band at 468.2 cm^{-1}, characteristic for Ce-O stretching band and a broad band at 704.3 cm^{-1} due to Ce-O-C mode, indicating the presence of CeO_2 [46, 47]. The bands at 1405 and 2975.2 cm^{-1} correspond to OH groups from physically adsorbed water [47].

DLS data indicate that CeNP have a hydrodynamic radius of 18 nm and a narrow size distribution. As the size of the CeNP is affecting its catalytic properties [48] a uniform distribution of the particles is required.

TEM images (Figure S2A) shows CeNP with a granular morphology, and a mean radius of (14 nm). The morphology of CeNP was was reported to affect their properties, nanorods and nanotubes exhibiting a higher catalytic activity than octahedral or grain- like CeNP [49]. However, as granular CeNPs were reported to exhibit more than 35% of the catalytic activity of nanorods [23], we used them for generation of nanoreactors because granular morphology is not expected to influence the self-assembly process of polymer vesicle formation.

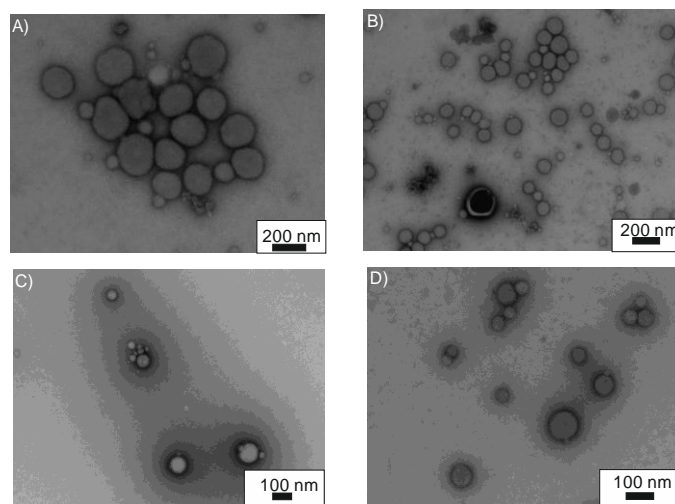### Morphology and size of empty and CeNP loaded PDMS-PNVP nanoreactors

Empty and CeNP loaded PDMS-PNVP polymer 3D assemblies were generated by self-assembly of PDMS-PNVP copolymers by the film rehydration method [50]. We characterized the 3D assemblies by a combination of light scattering and TEM. Light-scattering allows measuring the radii of gyration (R_g) and the hydrodynamic radius (R_h) of the self-assembled objects, while R_g/R_h (ρ-parameter) reveals the morphology of the 3D assemblies. Both PDMS-PNVP copolymers self-assembled in spherical supramolecular structures with R_g around 112 and 118 nm, and ρ values of 0.92 and 0.95 (Table 2). Values of the ρ-parameter are close to the expected values for hollow spheres (1.0), indicating that PDMS-PNVP copolymers self-assemble in vesicles. [51] For CeNP loaded supramolecular structures R_g values are 55 and 62 nm, respectively (Table 2). ρ values around 0.93-0.95, characteristic for hollow structures, indicates that the encapsulation of CeNP did not affect the self-assembly process, although it induced a decrease in the size of the vesicles.

Table 2. Light scattering data for empty and CeNP loaded PDMS-PNVP nanoreactors.

System	R_g / nm	R_h / nm	$\rho = R_g/R_h$
PDMS-PNVP1	112	121	0.92
PDMS-PNVP1-CeNP	55	59	0.93
PDMS-PNVP2	118	129	0.95
PDMS-PNVP2-CeNP	62	65	0.95

Figure 2. TEM micrographs of PDMS-PNVP polymersomes formed by self-assembly of block copolymers in PBS. (A) PDMS-PNVP1, (B) PDMS-PNVP2, (C) CeNP PDMS-PNVP1 based nanoreactor, (D) CeNP PDMS-PNVP2 based nanoreactor.

The smaller size of the PDMS-PNVP copolymers after loading with CeNP could be due to "guest influence" on the size of self-assembled structures. This has been previously observed for poly(ethylene oxide)-block-poly(butadiene) (PEO-PB) vesicles, where the encapsulation of horseradish peroxidase caused a transition from worm-like micelles (576 nm) to spherical polymersomes (147 nm) [52]. The same effect has also been shown with polystyrene-b-poly(isocyanoalanine(2-thiophen-3-yl-ethyl)amide) (PS-PIAT) vesicles, which, depending of the nature of the encapsulated guest, resulted in a decrease in size of polymersomes from 250 nm to 100 nm [53].

TEM was performed to visualize and compare the morphology and size of empty and CeNP loaded self-assembled structures. Spherical assemblies with radii of 80-120 nm were obtained for both tested copolymers in PBS buffer (Figure 2 A and B). Upon encapsulation of CeNP, both copolymers formed spherical assemblies with radii around 60 nm (Figure 2 C and D). The combination of LS and TEM data indicates that both selected copolymers, hydrated in the presence of CeNP, self-assemble into vesicles and encapsulate CeNP.

The final concentration of CeNP encapsulated in PDMS-PNVP nanoreactors was determined by UV-Vis spectroscopy as 0.074 mM CeNP for PDMS-PNVP1 vesicles and 0.064 mM for PDMS-PNVP2. Thus, encapsulation efficiencies of 74 and 64% respectively were obtained for an initial concentration of 0.1 mM CeNP. This is much higher than previously described for other antioxidant nanoreactors (23% for superoxide dismutase encapsulation [14] and 46% for copper superoxide dismutase mimics [9]. The probable number of CeNP per vesicle was identified as 2-3, for a medium diameter of 20 nm for CeNP. Encapsulation of CeNP inside nanoreactors prevents their aggregation, which is one of the main causes of toxicity [29].

Stability of PDMS-PNVP-CeNP nanoreactors over time and in the presence of hydrogen peroxide

Free CeNP (0.068 mM) aggregate and form larger structures of around 500 nm diameter after 6 hours in PBS (Figure S2 B), compared with 20 nm after 1 hour in PBS (Figure S2 A). In contrast, CeNP loaded PDMS-PNVP nanoreactors (containing 0.068 mM CeNP) are stable even after three months storage at room temperature, with TEM images indicating that their morphology and size were unchanged (Figure S3 A and B).

Reaction of CeNP with H_2O_2 is one of the leading causes of its toxicity. Thus the stability of CeNP loaded PDMS-PNVP nanoreactors in the presence of H_2O_2 was assessed by UV-vis spectroscopy. In the presence of H_2O_2, Ce^{3+}, which absorbs between 230 and 260 nm, is oxidized to Ce^{4+}, which absorbs in the 300-400 nm range, [19] and is then reduced back to Ce^{3+} [54]. Free CeNPs were reduced in the presence of H_2O_2 for 24 h (Figure 3 A), as shown by the decrease in the absorption peak at 320 nm for Ce^{4+}, whereas for CeNP in PDMS-PNVP nanoreactors the intensity of absorption peak at 320 nm was unchanged even after 24 h exposure to H_2O_2 (Figure 3 B and C). This indicates that the polymer membrane is impermeable

to H_2O_2 and that CeNP is completely protected inside the PDMS-PNVP nanoreactors.

Polymer membrane lack of permeability for H_2O_2 has already been shown in a previous study performed on horseradish peroxidase loaded PDMS-PNVP nanoreactors [40]. However, ROS penetrate the block copolymer membrane of such polymersomes [40].
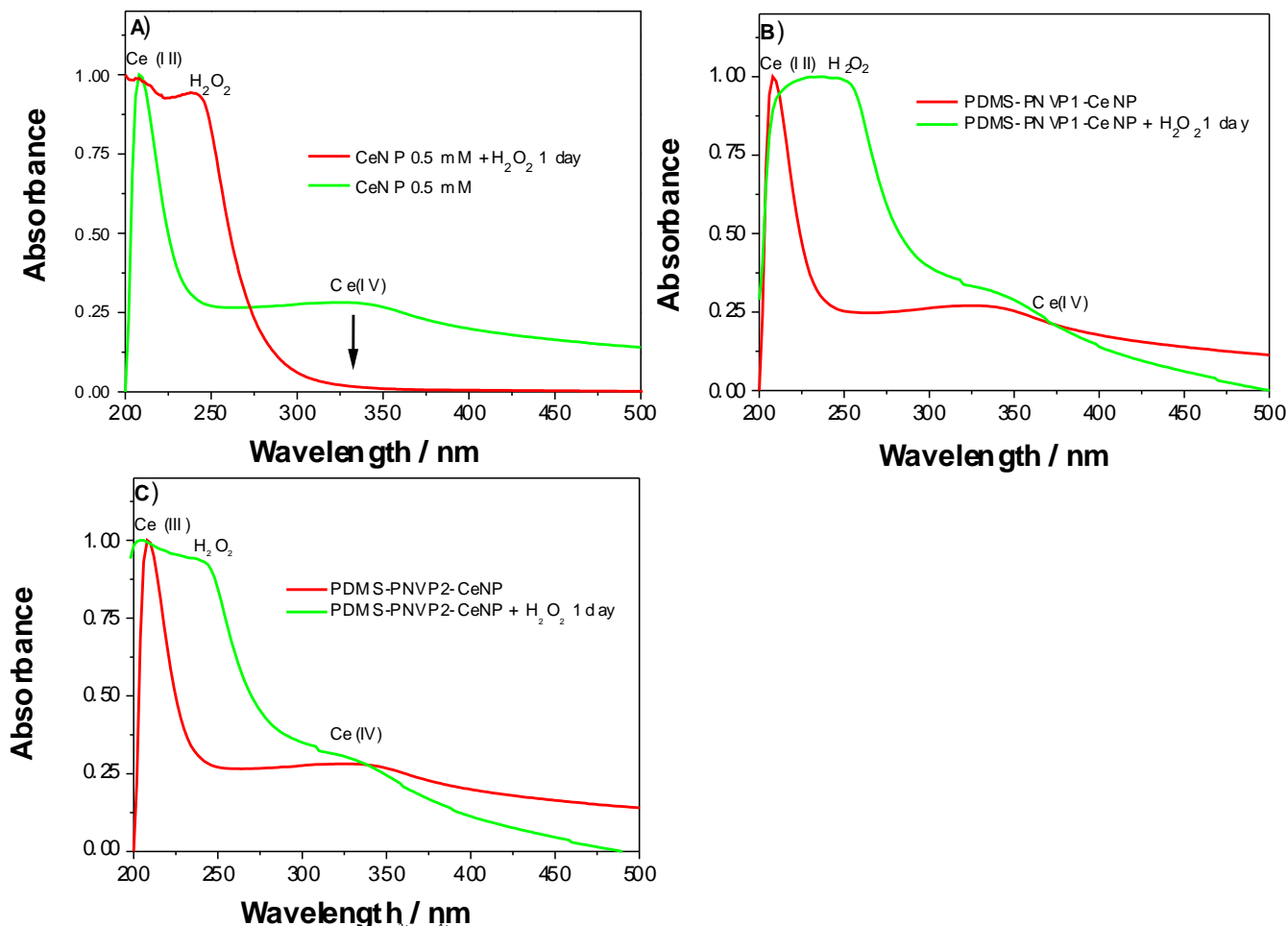

Figure 3. UV-vis spectra showing changes in the Ce^{3+}/Ce^{4+} ratios in the presence of hydrogen peroxide for: free CeNP (A), and encapsulated CeNP in nanoreactors based on PDMS-PNVP1 (B), and PDMS-PNVP2 (C), respectively.

Hydroxyl radical scavenging activity of CeNP and nanoreactors

The half-life of hydroxyl radicals (HO$^{\cdot}$) in solutions at room temperature is quite low (100 μs) [55], but their formation and decay can be investigated by spin trapping EPR, in which the addition reaction of a free radical to a spin trap forms a more stable spin adduct with paramagnetic parameters that depend on the nature of the trapped radical [56]. The characteristic DMPO/$^{\cdot}$OH spin adduct has a half-life of around 15 min [57], and its EPR spectrum consists of four lines with peak intensity ratios of 1:2:2:1 and hyperfine coupling constants a_N and a_H for ^{14}N and ^{1}H equal to 14.9 G (inset Figure 3A). Hydroxyl radicals were generated by a typical Fenton reaction involving Fe^{2+} and H_2O_2, [42] and their scavenging activity by CeNP was estimated by analyzing the plots (time scans) for DMPO/$^{\cdot}$OH adducts in the absence (control) and presence of different concentrations of CeNP (0.015 - 2.5 mM). Similar time scans were performed for PDMS-PNVP1 and PDMS-PNVP2 nanoreactors loaded respectively with 0.037 and 0.032 mM CeNP. Time scans of the intensity of the DMPO/$^{\cdot}$OH adduct in the absence or the presence of free CeNP or CeNP nanoreactors are presented in Figure 4.
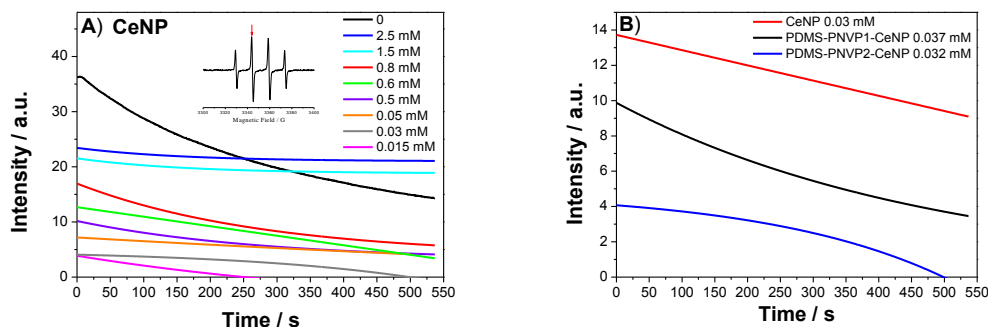
Journal Name

RSCPublishing

ARTICLE

Figure 4. (A) Decay of DMPO/·OH adducts at 298 K in the absence (0), and the presence of CeNP of various concentrations measured after 10 min of HO· generation. (B) Decay of DMPO/·OH adducts at 298 K in the presence of free CeNP (0.03 mM), and encapsulated CeNP in PDMS-PNVP1 and PDMS-PNVP2 nanoreactors after 10 min from the moment of HO· generation. The red downward arrow in the inset points to the monitored signal.

The intensity of DMPO/·OH adducts decreased drastically in the presence of CeNP (Figure 4A), and in addition a slight decrease in the adduct stability for various concentrations of CeNP is observed (Table 3). In the absence of CeNP (control), the time scans for the DMPO/·OH adduct show a significant decrease with time, and a half-life ($\tau_{1/2}$) of 960 s, which is similar to the reported value [48, 58].

Surprisingly, in the presence of 2.5 mM and 1.5 mM free CeNP the relative intensity of the DMPO/·OH adducts decreased, whereas the time scans did not, a result which suggests the continued generation of hydroxyl radicals. This represents the first evidence of the ability of CeNP to catalyse a Fenton-like reaction, although cerium chloride has been reported to catalyse a similar reaction [59]. A second spin trapping EPR experiment evaluated the ability of CeNP to generate hydroxyl radicals in the presence of hydrogen peroxide. In the presence of 5 mM CeNP a multicomponent EPR spectrum was recorded. This was deconvoluted into a typical signal for the DMPO/·OH adduct, a signal assigned to DMPO/·H adducts, and a three line signal corresponding to decomposition of DMPO (Figure 5A). A slightly different EPR spectrum, with significantly lower intensity, was observed in the presence of 0.03 mM CeNP (Figure 5B), indicating the ability of CeNP to generate radicals by a Fenton-like reaction over a broad concentration range. The difference between the EPR spectra is due to a higher CeNP concentration (over two order to magnitude), which induces changes both in the relative intensity of various adducts and their linewidth. XRD and FT-IR spectra of free CeNP (Figure S1 A and B) show only the characteristic patterns of CeO_2. As no pattern characteristic for iron oxide with (220), (311), (400), (331), (422), (511) and (440) reflections has been detected [60] it indicates no iron impurities in the system [61] (Figure S1A). In addition FT-IR spectrum of CeNP shows no characteristic

bands for iron 637 and 695 cm^{-1} [62] (Figure S1 B). The absence of iron characteristic band at 404 nm (in UV-vis spectrum Figure 3 A) indicate that no iron impurities were responsible for the Fenton like reaction induced by CeNP (if these impurities were present below the resolution limit of 0.01%).
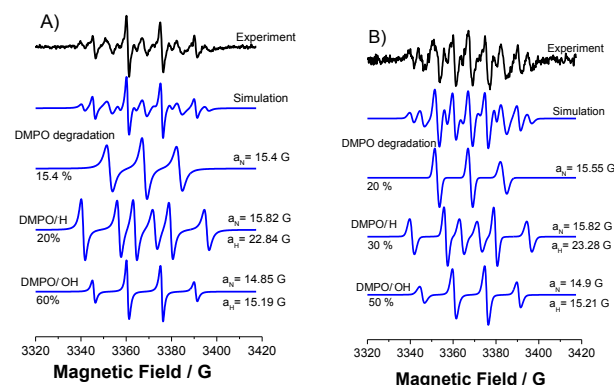

Figure 5. Experimental and simulated spectra of the multicomponent EPR signal obtained by spin trapping of the species formed in the reaction between hydrogen peroxide and 5 mM CeNP (A), and between hydrogen peroxide and 0.03 mM CeNP (B).

For lower CeNP concentrations (0.8 - 0.015 mM), the shapes of the decay profiles of the DMPO/·OH adducts (Figure 3A) were similar to those of the control with $\tau_{1/2}$ in the range 960 to 949 seconds (Table 3). A significant decrease in $\tau_{1/2}$ was observed only for 0.015 mM CeNP (747 seconds), which provides evidence of a significantly higher scavenging effect than the oxidation effect for CeNP (Fenton like reaction). The ability to scavenge hydroxyl radicals is inversely proportional the

concentration of CeNP, consistent with particle aggregation, [63] which resulted in a reduction of the number of catalytic sites

available for radical scavenging [48].

Table 3. $\tau_{1/2}$ for empty and CeNP-containing PDMS-PNVP vesicles.

[CeNP] /mM	0	0.8	0.6	0.5	0.05	0.03	0.015	PDMS-PNVP1-CeNP 0.037	PDMS-PNVP2-CeNP 0.032
$\tau_{1/2 /s}$	960	964	948	949	949	949	747	**804**	**927**

In the case of CeNP nanoreactors, the intensity of the DMPO/·OH signal recorded at the beginning of the measurement time was significantly higher than in the presence of the same concentration of CeNP (Figure 3B), while lower than in the absence of CeNP. This indicates a scavenging of hydroxyl radicals by CeNP-containing nanoreactors. The $\tau_{1/2}$ value (Table 3) decreased from 949 seconds for free CeNP to 927seconds for CeNP-containing PDMS-PNVP2 nanoreactors, and to 804 seconds for the CeNP-containing PDMS-PNVP1nanoreactors. This decrease is due to the blocking of the Fenton-like reaction by encapsulating the CeNP inside the polymeric vesicles [52], and the ability of encapsulated CeNP to scavenge hydroxyl radicals. Preventing aggregation of CeNP explains the faster decay of the DMPO/·OH signal with the encapsulated CeNP samples. The lower decrease of the $\tau_{1/2}$ value in the case of CeNP-containing PDMS-PNVP2 nanoreactors than for CeNP-containing PDMS-PNVP1 nanoreactors is due to the different CeNP encapsulation efficiency inside polymer vesicles.

Superoxide radical scavenging activity of CeNP, and CeNP-containing nanoreactors

DMPO is one of the most widely used spin traps for superoxide radical detection ($O_2^{\cdot-}$), but has a major disadvantage of a very short adduct half-life (of about one min [64]). In order to overcome the low stability of DMPO/·OOH adducts in aqueous solutions, a hypoxanthine – xanthine oxidase system (HX-XA) that is unaffected by the spin trap concentration [43] was used for constant and continuous generation of superoxide radicals. Maximum intensity of the DMPO/·OOH EPR spectrum was obtained after 10 min, and in order to assess the changes due to CeNP activity, and not to the signal decay induced by the DMPO/·OOH short half-life, EPR measurements were performed after 10 min incubation. In the absence of CeNP, a typical signal from the DMPO/·OOH adduct with a_N 14.12 G, $a_{H\beta}$ 11.34 G, and $a_{H\gamma}$ 1.59 G was obtained [43] (Figure 6A, No CeNP).
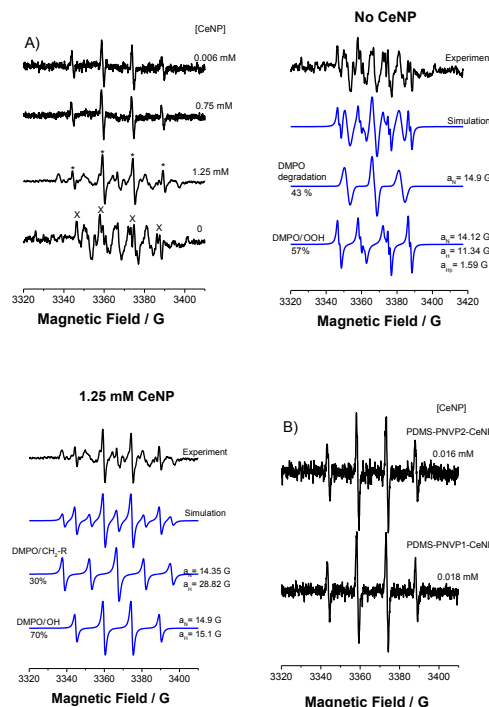

Figure 6. (A) CeNP scavenging activity for superoxide radicals of various concentrations of CeNP, from 1.25 mM to 0.006 mM, compared to the CeNP free control sample. Experimental and simulated EPR spectra of DMPO adducts in the absence (No CeNP), and in the presence of 1.25 mM CeNP (from figure 6A). (B) EPR spectra observed when superoxide radicals were generated by the HX-XA system in the presence of CeNP-containing PDMS-PNVP1 and CeNP-containing PDMS-PNVP2 nanoreactors.

In the presence of 1.25 mM CeNP, the characteristic EPR spectrum for DMPO/·OOH adducts was not detected, and instead a two component spectrum corresponding to OH (a_N 14.9 G, a_H 15.1 G) C-centred radical adducts were observed (DMPO/CH$_2$-R) [56]. The presence of CeNP seems to favour the formation of DMPO C-centred radical adduct, while in the absence of CeNP a typical aminoxy signal was detected [56]. The DMPO/·OH adduct signal was detected at concentrations of CeNP up to 0.006 mM, indicating a preference of CeNP to scavenge superoxide radicals, in agreement with reported data [19]. As the superoxide radicals are generated in a continuous manner in the system, the disappearance of the DMPO/·OOH adducts can be related only with the scavenging ability of

CeNP, as already reported [48]. Similarly, CeNP containing nanoreactors induced the disappearance of DMPO/·OOH signal (Figure 6B), due to their ability to efficiently scavenge superoxide radicals.

In conclusion, spin trapping EPR indicates that CeNP loaded in PDMS-PNVP nanoreactors have a high scavenging activity for both hydroxyl and superoxide radicals, whilst showing no ability to generate ROS because of their membrane impermeability to hydrogen peroxide.

Cellular uptake and cytotoxicity of CeNP-containing nanoreactors

The internalization, stability, and cytotoxicity of CeNP-containing nanoreactors were tested on HeLa cells. To investigate their uptake and stability inside cells, nanoreactors co-encapsulating CeNP and doxorubicin were prepared in similar conditions to those containing only CeNP. Doxorubicin was selected due to its ability to intercalate with cellular DNA when released in cells, and the overlying of fluorescence signals from doxorubicin and DNA stained with Hoechst [65,66]. CeNP- and doxorubicin-containing nanoreactors (as seen from the UV-vis spectra measured after purification; data not shown) were up-taken by cells (Figure 7 A-A3 and B-B3), irrespective of the PDMS-PNVP molecular weight.
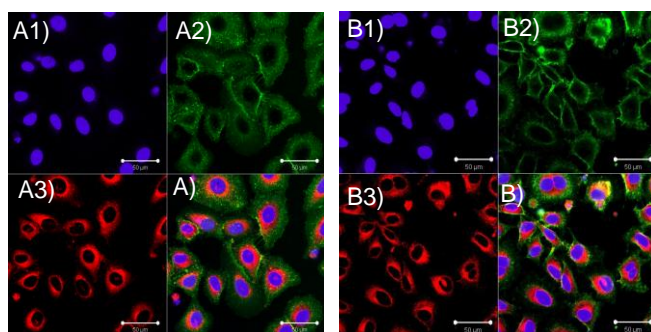

Figure 7. HeLa cells incubated for 24 h with co-encapsulated CeNP and doxorubicin in PDMS-PNVP1 vesicles (0.0036 mM CeNP) (A), and in PDMS-PNVP2 vesicles (0.003mM CeNP) (B). Violet channel: Hoechst DNA staining (A1, B1), green channel: Cell Mask Deep Red staining (A2, B2), and red channel: doxorubicin loaded vesicles (A3, B3).

The fluorescence signal of doxorubicin did not significantly overlap the nucleus fluorescence signal, suggesting that the majority of nanoreactors remained intact after being taken up by HeLa cells. In addition, flow cytometry with doxorubicin- and CeNP-containing nanoreactors confirmed their uptake after 24 h (Figure 8 A). The shifts of the peaks corresponding to CeNP-containing nanoreactors compared to the normal cells after 24 h, and 72 h (Figure 8 B), respectively indicate that PDMS-PNVP2 nanoreactors have higher uptake ability than PDMS-PNVP1 nanoreactors.
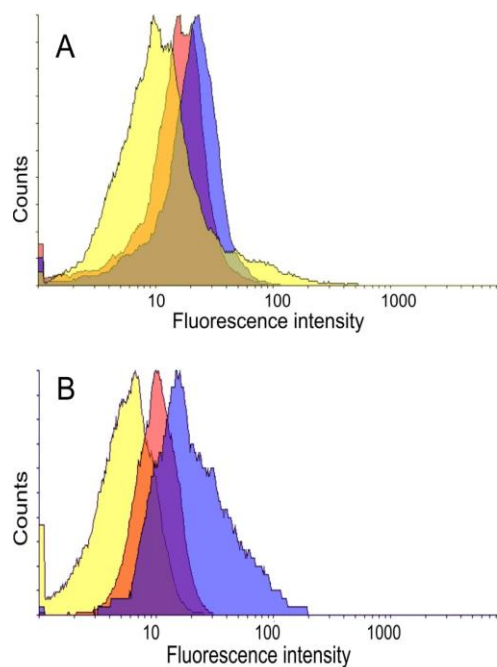

Figure 8. Flow cytometry analysis of HeLa cells incubated without nanoreactors (yellow), and in the presence of CeNP- and doxorubicin-containing PDMS-PNVP1 nanoreactors (red), and PDMS-PNVP2 nanoreactors (blue) for an incubation time 24 h (A), and an incubation time of 72h (B).

In order to evaluate the cytotoxicity of CeNP-containing nanoreactors, HeLa cells were incubated with CeNP, and CeNP-containing nanoreactors for 24 h, and 72h respectively. Cytotoxicity was assessed with the MTS assay. After 24 h incubation, free CeNPs were shown to be slightly cytotoxic (around 30% cell death), whereas CeNP-containing nanoreactors had almost no toxicity (Figure 9A). With a longer term exposure (72 h), the cytotoxicity of free CeNP was significantly higher (especially for concentrations > 10 µg/mL), with cell death reaching 51% (Figure 9B), in agreement with reported data [31,33]. In contrast, after 72 h incubation the CeNP-containing PDMS-PNVP1 nanoreactors showed cytotoxicity of around 10% while the cell death with the PDMS-PNVP2 nanoreactors was about 30% (Figure 9B). The decrease in cell viability in the presence of the nanoreactors might be the result of small number of vesicles breaking during 72 h incubation time. This effect is extremely small for PDMS-PNVP1 nanoreactors (10% cell death) compared with PDMS-PNVP2 nanoreactors (30% cells death) for the same concentration of CeNP (51% cells death).
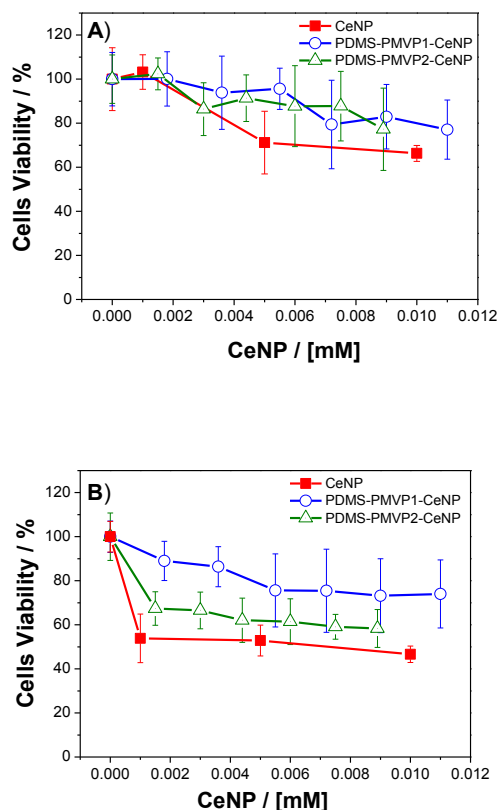
Nanoscale Accepted Manuscript

Figure 10. Viability of HeLa cells after 24 h. 1) Control cells; 2) HeLa cells exposed to paraquat; 3) HeLa cells exposed to paraquat in the presence of 0.004 M CeNP-containing PDMS-PNVP1 nanoreactors; 4) HeLa cells exposed to paraquat in presence of 0.004 M CeNP-containing PDMS-PNVP2 nanoreactors; 5) HeLa cells exposed to paraquat in presence of free 0.004 M CeNP.

Figure 9. HeLA cell viability after incubation with free CeNP, and encapsulated CeNP in nanoreactors for (A) 24h, and (B) 72 h.

No toxicity of the PDMS-PNVP polymer vesicles on HeLa cells was observed after 24 h or 72 h exposure, even at significantly higher polymer concentrations than that used to obtain nanoreactors (5 mg/mL), as shown for 50 mg/mL polymer (Figure S4).

In order to investigate the intracellular activity of CeNP-containing nanoreactors, cells were exposed to oxidative stress induced by addition of paraquat. After exposure to ROS, cells were analysed by PI staining, and flow cytometry to determine the viability [7]. The viability of HeLa cells decreased to 60% after 24 hours incubation in the presence of paraquat. In contrast, the viability of HeLa cells pre-treated with CeNP-containing nanoreactors or free CeNP and then with paraquat remained at a high level of around 85% for PDMS-PNVP2 nanoreactors, and 96% for PDMS-PNVP1 ones, compared with the situation of incubation with free CeNP 0.004 mM 96% (Figure 10). The cell toxicity in the presence of paraquat and CeNP loaded nanoreactors (Figure 10) is higher than the toxicity of CeNP containing nanoreactors alone shown in Figure 9 A. This represents a clear proof that inside cells CeNP-containing nanoreactors act as an efficient ROS detoxification system.
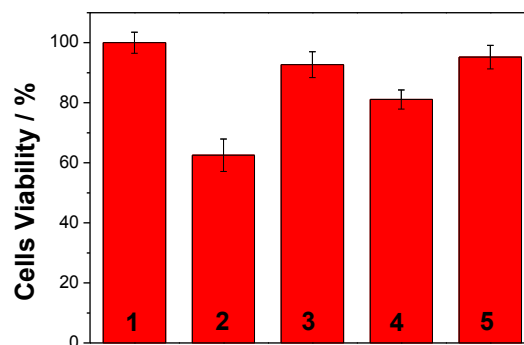
Conclusions

CeNP-containing nanoreactors were engineered by encapsulation of CeNP inside vesicles generated by self-assembly of PDMS-PNVP triblock copolymers under physiological pH conditions. Spin trapping EPR established that CeNP have a dual activity, involving both scavenging and generation of reactive oxygen species in the presence of hydrogen peroxide. In contrast, CeNP loaded nanoreactors benefit from polymer membrane protection, which blocks access of hydrogen peroxide to the inner cavity where CeNP are located, and therefore exhibit only an efficient scavenging activity for both hydroxyl and superoxide radicals. Upon encapsulation, the nanorectors prevent the aggregation of CeNP, and the Fenton-like reaction with hydrogen peroxide, which are known to be the main reasons for CeNP toxicity. CeNP nanoreactors were taken up by HeLa cells, and showed almost no cytotoxicity, even after long incubation times. In addition, inside nanoreactors CeNP preserved their superantioxidant activity, for both hydroxyl and superoxide radicals. Indeed, inside cells exposed to oxidative stress CeNP-containing nanoreactors were effective in ROS scavenging because of the regenerative redox chemistry of loaded CeNP. Compared to free CeNP, which induces significant cytotoxicity, CeNP-containing nanoreactors possess high superantioxidant activity, long term stability, and almost no toxicity. Our strategy for engineering CeNP-containing nanoreactors represents a straightforward solution to reducing CeNP toxicity whilst preserving their functionality, and serving to offer the nanoreactors as an efficient solution to fighting oxidative stress in a large variety of domains, ranging from medicine to environmental protection.

Acknowledgements

Basel, and this is gratefully acknowledged. MS acknowledges G. Persy (University of Basel), and V. Olivieri (Microscopy Center, University of Basel) for TEM-measurements. MS thanks Prof. C. De Capitani, University of Basel, for XRD-measurements. Authors thank Dr. B.A. Goodman for editing the manuscript.

Notes and references

[a] Department of chemistry, University of Basel, Klingelbergstrasse 80, CH-4056 Basel, Switzerland. Fax: +41(0)61 267 3850; Tel: +41 (0)61 267 3839; E-mail: Cornelia.Palivan@unibas.ch.

† Electronic Supplementary Information (ESI) available: [Additional information including TEM images of the CeNP aggregation in time, the stability of nanoreactors loaded with CeNP and the toxicity of the PDMS-PNVP copolymers are presented in the supporting information]. See DOI: 10.1039/b000000x/

1. Chen, D.; Xi, T.; Bai, J., Biological effects induced by nanosilver particles: in vivo study. *Biomed Mater* **2007,** *2* (3), S126-8.

2. Gaynor, J. D.; Karakoti, A. S.; Inerbaev, T.; Sanghavi, S.; Nachimuthu, P.; Shutthanandan, V.; Seal, S.; Thevuthasan, S., Enzyme-free detection of hydrogen peroxide from cerium oxide nanoparticles immobilized on poly(4-vinylpyridine) self-assembled monolayers. *Journal of Materials Chemistry B* **2013,** *1* (28), 3443-3450.

3. Wason, M. S.; Zhao, J. H., Cerium oxide nanoparticles: potential applications for cancer and other diseases. *Am J Transl Res* **2013,** *5* (2), 126-131.

4. Onaca, O.; Hughes, D. W.; Balasubramanian, V.; Grzelakowski, M.; Meier, W.; Palivan, C. G., SOD Antioxidant Nanoreactors: Influence of Block Copolymer Composition on the Nanoreactor Efficiency. *Macromol Biosci* **2010,** *10* (5), 531-538.

5. Axthelm, F.; Casse, O.; Koppenol, W. H.; Nauser, T.; Meier, W.; Palivan, C. G., Antioxidant nanoreactor based on superoxide dismutase encapsulated in superoxide-permeable vesicles. *J Phys Chem B* **2008,** *112* (28), 8211-7.

6. Dobrunz, D.; Toma, A. C.; Tanner, P.; Pfohl, T.; Palivan, C. G., Polymer Nanoreactors with Dual Functionality: Simultaneous Detoxification of Peroxynitrite and Oxygen Transport. *Langmuir* **2012,** *28* (45), 15889-15899.

7. Tanner, P.; Balasubramanian, V.; Palivan, C. G., Aiding Nature's Organelles: Artificial Peroxisomes Play Their Role. *Nano Letters* **2013,** *13* (6), 2875-2883.

8. Louzao, I.; van Hest, J. C. M., Permeability Effects on the Efficiency of Antioxidant Nanoreactors. *Biomacromolecules* **2013,** *14* (7), 2364-2372.

9. Balasubramanian, V.; Onaca, O.; Ezhevskaya, M.; Van Doorslaer, S.; Sivasankaran, B.; Palivan, C. G., A surprising system: polymeric nanoreactors containing a mimic with dual-enzyme activity. *Soft Matter* **2011,** *7* (12), 5595-5603.

10. Peters, R. J. R. W.; Louzao, I.; van Hest, J. C. M., From polymeric nanoreactors to artificial organelles. *Chem Sci* **2012,** *3* (2), 335-342.

11. Velázquez, M. M.; Valero, M.; Ortega, F., Spontaneous Vesicles Modulated by Polymers. *Polymers* **2011,** *3* (3), 1255-1267.

12. Tanner, P.; Baumann, P.; Enea, R.; Onaca, O.; Palivan, C.; Meier, W., Polymeric vesicles: from drug carriers to nanoreactors and artificial organelles. *Acc Chem Res* **2011,** *44* (10), 1039-49.

13. Brinkhuis, R. P.; Rutjes, F. P. J. T.; van Hest, J. C. M., Polymeric vesicles in biomedical applications. *Polymer Chemistry* **2011,** *2* (7), 1449-1462.

14. Onaca, O.; Hughes, D. W.; Balasubramanian, V.; Grzelakowski, M.; Meier, W.; Palivan, C. G., SOD antioxidant nanoreactors: influence of block copolymer composition on the nanoreactor efficiency. *Macromol Biosci* **2010,** *10* (5), 531-8.

15. Baumann, P.; Balasubramanian, V.; Onaca-Fischer, O.; Sienkiewicz, A.; Palivan, C. G., Light-responsive polymer nanoreactors: a source of reactive oxygen species on demand. *Nanoscale* **2013,** *5* (1), 217-224.

16. Redoules, D.; Perie, J.; Viode, C.; Mavon, A.; Fournier, D.; Daunes, S.; Casas, C.; Lougarre, A.; De Viguerie, N., Slow Internal Release of Bioactive Compounds Under the Effect of Skin Enzymes. *J Investig Dermatol* **2005,** *125* (2), 270-277.

17. Wang, X.; Lv, L.; Zhang, Q.; Zhang, Y.; Wang, J.; Shen, M., The different NOx trap performance on ceria and barium/ceria containing LNT catalysts below 200 [degree]C. *Catalysis Science & Technology* **2013,** *3* (1), 200-207.

18. Merrifield, R. C.; Wang, Z. W.; Palmer, R. E.; Lead, J. R., Synthesis and Characterization of Polyvinylpyrrolidone Coated Cerium Oxide Nanoparticles. *Environ Sci Technol* **2013,** *47* (21), 12426-12433.

19. Heckert, E. G.; Karakoti, A. S.; Seal, S.; Self, W. T., The role of cerium redox state in the SOD mimetic activity of nanoceria. *Biomaterials* **2008,** *29* (18), 2705-9.

20. Si, R.; Zhang, Y.-W.; Li, S.-J.; Lin, B.-X.; Yan, C.-H., Urea-Based Hydrothermally Derived Homogeneous Nanostructured Ce1-xZrxO2 (x = 0−0.8) Solid Solutions: A Strong Correlation between Oxygen Storage Capacity and Lattice Strain. *The Journal of Physical Chemistry B* **2004,** *108* (33), 12481-12488.

21. Dowding, J.; Seal, S.; Self, W., Cerium oxide nanoparticles accelerate the decay of peroxynitrite (ONOO−). *Drug Deliv Transl Res* **2013,** *3* (4), 375-379.

22. Xue, Y.; Luan, Q.; Yang, D.; Yao, X.; Zhou, K., Direct Evidence for Hydroxyl Radical Scavenging Activity of Cerium Oxide Nanoparticles. *The Journal of Physical Chemistry C* **2011,** *115* (11), 4433-4438.

23. Zhang, F.; Chan, S. W.; Spanier, J. E.; Apak, E.; Jin, Q.; Robinson, R. D.; Herman, I. P., Cerium oxide nanoparticles: Size-selective formation and structure analysis. *Appl Phys Lett* **2002,** *80* (1), 127-129.

24. Heckman, K. L.; DeCoteau, W.; Estevez, A.; Reed, K. J.; Costanzo, W.; Sanford, D.; Leiter, J. C.; Clauss, J.; Knapp, K.; Gomez, C.; Mullen, P.; Rathbun, E.; Prime, K.; Marini, J.; Patchefsky, J.; Patchefsky, A. S.; Hailstone, R. K.; Erlichman, J. S., Custom Cerium Oxide Nanoparticles Protect against a Free Radical Mediated Autoimmune Degenerative Disease in the Brain. *ACS Nano* **2013**.

25. Kamada, K.; Horiguchi, K.; Hyodo, T.; Shimizu, Y., Photochemical Synthesis of Monodispersed Ceria Nanocrystals in Simple Cerium Nitrate Solution without Additives. *Cryst Growth Des* **2011,** *11* (4), 1202-1207.

26. Schubert, D.; Dargusch, R.; Raitano, J.; Chan, S. W., Cerium and yttrium oxide nanoparticles are neuroprotective. *Biochem Biophys Res Commun* **2006,** *342* (1), 86-91.

27. Asati, A.; Santra, S.; Kaittanis, C.; Perez, J. M., Surface-Charge-Dependent Cell Localization and Cytotoxicity of Cerium Oxide Nanoparticles. *ACS Nano* **2010,** *4* (9), 5321-5331.

28. Amin, K. A.; Hassan, M. S.; Awad, E. T.; Hashem, K. S., The protective effects of cerium oxide nanoparticles against hepatic oxidative damage induced by monocrotaline. *Int J Nanomedicine* **2011,** *6*, 143-149.

29. Zhang, H. F.; He, X. A.; Zhang, Z. Y.; Zhang, P.; Li, Y. Y.; Ma, Y. H.; Kuang, Y. S.; Zhao, Y. L.; Chai, Z. F., Nano-CeO2 Exhibits Adverse Effects at Environmental Relevant Concentrations. *Environ Sci Technol* **2011,** *45* (8), 3725-3730.

30. Mahmoudi, M.; Azadmanesh, K.; Shokrgozar, M. A.; Journeay, W. S.; Laurent, S., Effect of Nanoparticles on the Cell Life Cycle. *Chem Rev* **2011,** *111* (5), 3407-3432.

31. Park, E. J.; Choi, J.; Park, Y. K.; Park, K., Oxidative stress induced by cerium oxide nanoparticles in cultured BEAS-2B cells. *Toxicology* **2008,** *245* (1-2), 90-100.

32. Celardo, I.; Pedersen, J. Z.; Traversa, E.; Ghibelli, L., Pharmacological potential of cerium oxide nanoparticles. *Nanoscale* **2011,** *3* (4), 1411-1420.

33. De Marzi, L.; Monaco, A.; De Lapuente, J.; Ramos, D.; Borras, M.; Di Gioacchino, M.; Santucci, S.; Poma, A., Cytotoxicity and Genotoxicity of Ceria Nanoparticles on Different Cell Lines in Vitro. *Int J Mol Sci* **2013,** *14* (2), 3065-3077.

34. Courbiere, B.; Auffan, M.; Rollais, R.; Tassistro, V.; Bonnefoy, A.; Botta, A.; Rose, J.; Orsière, T.; Perrin, J., Ultrastructural Interactions and Genotoxicity Assay of Cerium Dioxide Nanoparticles on Mouse Oocytes. *Int J Mol Sci* **2013,** *14* (11), 21613-21628.

35. Nalabotu, S. K.; Kolli, M. B.; Triest, W. E.; Ma, J. Y.; Manne, N. D. P. K.; Katta, A.; Addagarla, H. S.; Rice, K. M.; Blough, E. R., Intratracheal instillation of cerium oxide nanoparticles induces hepatic toxicity in male Sprague-Dawley rats. *Int J Nanomedicine* **2011,** *6*, 2327-2335.

36. Aalapati, S.; Ganapathy, S.; Manapuram, S.; Anumolu, G.; Prakya, B. M., Toxicity and bio-accumulation of inhaled cerium oxide nanoparticles in CD1 mice. *Nanotoxicology 0* (0), 1-13.

37. Ozel, R. E.; Hayat, A.; Wallace, K. N.; Andreescu, S., Effect of cerium oxide nanoparticles on intestinal serotonin in zebrafish. *RSC Advances* **2013,** *3* (35), 15298-15309.

38. Balasubramanian, V.; Onaca, O.; Enea, R.; Hughes, D. W.; Palivan, C. G., Protein delivery: from conventional drug delivery carriers to polymeric nanoreactors. *Expert Opin Drug Deliv* **2010,** *7* (1), 63-78.

39. Epure, V.; Ioan, S.; Pinteala, M.; Harabagiu, V.; Simionescu, B. C.; Simionescu, B. C., Viscometric study of poly(dimethylsiloxaneb-N-vinylpyrrolidone) in water solutions. *High Perform Polym* **2005,** *17* (2), 251-261.

40. Spulber, M.; Baumann, P.; Saxer, S. S.; Pieles, U.; Meier, W. P.; Bruns, N., Poly(N-vinylpyrrolidone)-poly(dimethylsiloxane)-based polymersome nanoreactors for laccase-catalyzed biotransformations. *Biomacromolecules* **2014**.

41. Battaglia, G.; Ryan, A. J., Pathways of Polymeric Vesicle Formation. *The Journal of Physical Chemistry B* **2006,** *110* (21), 10272-10279.

42. Lloyd, R. V.; Hanna, P. M.; Mason, R. P., The origin of the hydroxyl radical oxygen in the Fenton reaction. *Free Radic Biol Med* **1997,** *22* (5), 885-8.

43. Clement, J. L.; Ferre, N.; Siri, D.; Karoui, H.; Rockenbauer, A.; Tordo, P., Assignment of the EPR spectrum of 5,5-dimethyl-1-pyrroline N-oxide (DMPO) superoxide spin adduct. *J Org Chem* **2005,** *70* (4), 1198-203.

44. http://www.niehs.nih.gov/research/resources/software/tools/index.cfm.

45. Balakrishnan, G.; Raghavan, C. M.; Ghosh, C.; Divakar, R.; Mohandas, E.; Song, J. I.; Bae, S. I.; Kim, T. G., X-ray diffraction, Raman and photoluminescence studies of nanocrystalline cerium oxide thin films. *Ceram Int* **2013,** *39* (7), 8327-8333.

46. Dos Santos, M. L.; Lima, R. C.; Riccardi, C. S.; Tranquilin, R. L.; Bueno, P. R.; Varela, J. A.; Longo, E., Preparation and characterization of ceria nanospheres by microwave-hydrothermal method. *Mater Lett* **2008,** *62* (30), 4509-4511.

47. Renu, G.; Rani, V. V. D.; Nair, S. V.; Subramanian, K. R. V.; Lakshmanan, V.-K., Development of Cerium Oxide Nanoparticles and Its Cytotoxicity in Prostate Cancer Cells. *Advanced Science Letters* **2012,** *6* (1), 17-25.

48. Babu, S.; Velez, A.; Wozniak, K.; Szydlowska, J.; Seal, S., Electron paramagnetic study on radical scavenging properties of ceria nanoparticles. *Chem Phys Lett* **2007,** *442* (4-6), 405-408.

49. Ta, N.; Liu, J.; Shen, W., Tuning the shape of ceria nanomaterials for catalytic applications. *Chinese Journal of Catalysis* **2013,** *34* (5), 838-850.

50. Battaglia, G.; Ryan, A. J.; Tomas, S., Polymeric vesicle permeability: a facile chemical assay. *Langmuir* **2006,** *22* (11), 4910-3.

51. Stauch, O.; Schubert, R.; Savin, G.; Burchard, W., Structure of artificial cytoskeleton containing liposomes in aqueous solution studied by static and dynamic light scattering. *Biomacromolecules* **2002,** *3* (3), 565-78.

52. Spulber, M.; Najer, A.; Winkelbach, K.; Glaied, O.; Waser, M.; Pieles, U.; Meier, W.; Bruns, N., Photoreaction of a Hydroxyalkyphenone with the Membrane of Polymersomes: A Versatile Method To Generate Semipermeable Nanoreactors. *J Am Chem Soc* **2013,** *135* (24), 9204-9212.

53. Kuiper, S. M.; Nallani, M.; Vriezema, D. M.; Cornelissen, J. J.; van Hest, J. C.; Nolte, R. J.; Rowan, A. E., Enzymes containing porous polymersomes as nano reaction vessels for cascade reactions. *Org Biomol Chem* **2008,** *6* (23), 4315-8.

54. Sworski, T. J.; Mahlman, H. A.; Matthews, R. W., Reduction of cerium(IV) by hydrogen peroxide. Dependence of reaction rate on Hammett's acidity function. *The Journal of Physical Chemistry* **1971,** *75* (2), 250-255.

55. Rudolph, R.; Francke, K. P.; Miessner, H., OH Radicals as Oxidizing Agent for the Abatement of Organic Pollutants in Gas Flows by Dielectric Barrier Discharges. *Plasmas and Polymers* **2003,** *8* (2), 153-161.

56. Buettner, G. R., Spin trapping: ESR parameters of spin adducts. *Free Radic Biol Med* **1987,** *3* (4), 259-303.

57. Spulber, M.; Schlick, S., Using Cyclodextrins to Encapsulate Oxygen-Centered and Carbon-Centered Radical Adducts: The Case of DMPO, PBN, and MNP Spin Traps. *Journal of Physical Chemistry A* **2010,** *114* (21), 6217-6225.

58. Spulber, M.; Schlick, S., Using cyclodextrins to encapsulate oxygen-centered and carbon-centered radical adducts: the case of DMPO, PBN, and MNP spin traps. *J Phys Chem A* **2010,** *114* (21), 6217-25.

59. Heckert, E. G.; Seal, S.; Self, W. T., Fenton-like reaction catalyzed by the rare earth inner transition metal cerium. *Environ Sci Technol* **2008,** *42* (13), 5014-9.

60. Mahadevan, S.; Behera, S. P.; Gnanaprakash, G.; Jayakumar, T.; Philip, J.; Rao, B. P. C., Size distribution of magnetic iron oxide

Nanoscale Accepted Manuscript

nanoparticles using Warren–Averbach XRD analysis. *Journal of Physics and Chemistry of Solids* **2012,** *73* (7), 867-872.

61. Varasteh, M.; Deng, Z.; Hwang, H.; Kim, Y. J.; Wong, G. B., Quantitative determination of polymorphic impurity by X-ray powder diffractometry in an OROS® formulation. *Int J Pharm* **2009,** *366* (1–2), 74-81.

62. Guo, Z. H.; Lei, K.; Li, Y. T.; Ng, H. W.; Prikhodko, S.; Hahn, H. T., Fabrication and characterization of iron oxide nanoparticles reinforced vinyl-ester resin nanocomposites. *Compos Sci Technol* **2008,** *68* (6), 1513-1520.

63. Pyrgiotakis, G.; Blattmann, C. O.; Pratsinis, S.; Demokritou, P., Nanoparticle-nanoparticle interactions in biological media by atomic force microscopy. *Langmuir* **2013,** *29* (36), 11385-95.

64. Villamena, F. A., Superoxide Radical Anion Adduct of 5,5-Dimethyl-1-pyrroline N-Oxide. 5. Thermodynamics and Kinetics of Unimolecular Decomposition. *Journal of Physical Chemistry A* **2009,** *113* (22), 6398-6403.

65. Chen, N. T.; Wu, C. Y.; Chung, C. Y.; Hwu, Y.; Cheng, S. H.; Mou, C. Y.; Lo, L. W., Probing the Dynamics of Doxorubicin-DNA Intercalation during the Initial Activation of Apoptosis by Fluorescence Lifetime Imaging Microscopy (FLIM). *Plos One* **2012,** *7* (9).

66. Tacar, O.; Sriamornsak, P.; Dass, C. R., Doxorubicin: an update on anticancer molecular action, toxicity and novel drug delivery systems. *J Pharm Pharmacol* **2013,** *65* (2), 157-170.

Nanoscale Accepted Manuscript